Isomorphous Substitution of Gallium into MFI-Framework Zeolite Increases 2,5-Dimethylfuran to Aromatics Selectivity and Suppresses

Topics in Catalysis
https://doi.org/10.1007/s11244-022-01776-2

ORIGINAL PAPER

Isomorphous Substitution of Gallium into MFI-Framework Zeolite Increases 2,5-Dimethylfuran to Aromatics Selectivity and Suppresses Catalyst Deactivation

Christopher Sauer[1] · **Guido J. L. de Reijer**[1] · **Andreas Schaefer**[1] · **Per-Anders Carlsson**[1]

Accepted: 15 December 2022

Abstract
The valorization of biomass-derived molecules into commodity chemicals is important for the transition to renewable feedstocks. The model platform molecule 2,5-dimethylfuran (2,5-dmf) can be converted into value-added aromatics such as benzene, toluene, and xylenes (BTX) over zeolite catalysts. To explore the role of the zeolite acid site(s) in BTX selectivity, gallium has been isomorphously substituted into the framework, resulting in a Ga-silicate. Compared to the ZSM-5 counterpart, this modification shows enhanced benzene selectivity as well as resistance to deactivation by coke in continuous catalytic performance tests.

Keywords 2,5-Dimethylfuran · Zeolite · Aromatics · Gallium · Ga-silicate · Biomass conversion

1 Introduction

The urgent need to phase out of fossil resources for our energy demands also pushes the chemical industry to find alternative feedstocks for the sustainable production of high-volume commodity chemicals. Besides plastic waste, biomass and biomass waste products are often considered such alternatives [1–3]. Biomass is a renewable – and potentially sustainable – carbon source if the protection of local communities, biodiversity, and local ecosystems is ensured [4, 5]. It can be converted by catalytic fast pyrolysis (CFP) which offers a potential route to make benzene, toluene, and xylenes [6]. These compounds, often abbreviated BTX, form one of the important groups of commodity chemicals. For this purpose, zeolites have been studied extensively thanks to their favorable properties including high thermal stability, high surface area, shape-selectivity, and tunability of elemental composition [7]. For the production of aromatics, MFI-framework zeolites such as ZSM-5 have shown high selectivity [8]. However, the selectivity obtained in continuous operation, i.e. when using chemical flow reactors instead of batch or semi-batch reactors, still requires improvement to become more attractive industrially. Furthermore, the ZSM-5 catalyst often suffers from rapid deactivation due to coking [9].

Many attempts to increase the formation of aromatics by modification of the catalyst properties have been made, e.g., by introducing metals such as Zn [10–12], Ga [11–13] or by introducing mesopores through desilication [14]. In this regard, gallium modification of zeolites seems to yield promising results. For example, H-ZSM-5 that was ion-exchanged and impregnated with gallium to form Ga-ZSM-5 with extra-framework gallium species shows higher BTX selectivity [11, 13, 15, 16]. For aluminium containing zeolites, another type of metal species has been identified, namely framework associated aluminium [17]. In a similar way, gallium introduced into ZSM-5 can result in framework associated gallium. Its synergistic interaction with framework Al results in a dual-function and promotes aromatization, sometimes

Guido J. L. de Reijer and Christopher Sauer have contributed equally to this work.

✉ Christopher Sauer
sauerc@chalmers.se

Guido J. L. de Reijer
guidod@chalmers.se

Andreas Schaefer
andreas.schaefer@chalmers.se

Per-Anders Carlsson
per-anders.carlsson@chalmers.se

[1] Department of Chemistry and Chemical Engineering, Chalmers University of Technology, Gothenburg 41 296, Sweden

Published online: 28 December 2022

illustrated by a decrease in Brønsted/Lewis acid site ratio [16, 18]. Besides extra-framework and framework associated gallium, there are indications that gallium in framework positions can enhance production of aromatics in co-fed CFP of biomass and low-density polyethylene [19], as well as increase selectivity towards monoaromatic compounds [20].

However, the role of gallium in biomass aromatization is not yet fully understood. To address this, experimental studies designed to utilize model compounds and pure Ga-silicates without any aluminium have the potential to acquire new knowledge about the catalytic function of the acid sites. Since Si-O(H)-Ga sites are more covalent than their aluminium derivatives, their Brønsted acid strength is slightly reduced [21], offering the potential for more selective reactions.

In this work, we investigate Ga-silicate for the production of BTX aromatics from 2,5-dmf using a continuous chemical flow reactor. We apply an on-line analysis of the effluent product stream using the combination of Fourier-transform infrared spectroscopy (FTIR) and mass spectrometry (MS) analysis, which offers a high time resolution [22, 23]. The results are compared with those obtained for two H-ZSM-5 catalysts as well as Silicalite-1. We observe increased benzene selectivity for the Ga-silicate. Further, catalytic activity towards BTX aromatics is prolonged compared to ZSM-5. Moreover, lower acid site density seems to be advantageous for suppressed deactivation, leading to long-lasting activity for isomerization of the reactant.

2 Experimental

2.1 Catalyst Materials

The following materials were used as catalysts: commercially available H-ZSM-5 (AkzoNobel, Si/Al=11, further noted as ZSM-5(11)), H-ZSM-5 (Si/Al=41, further noted as ZSM-5(41)), Silicalite-1 and Ga-silicate. The latter three were prepared as described elsewhere [24] following the method by Szotak et al [25]. In short, tetraethyl orthosilicate was hydrolyzed in water and oxalic acid (pH 2), followed by the addition of gallium nitrate hydrate or sodium aluminate to synthesize Ga-silicate or H-ZSM-5 respectively. Then, 1.0 M tetrapropylammonium hydroxide was added and the pH was adjusted by adding 1M NaOH solution (to pH = 11). The gels were heated in unstirred autoclaves for 5 days at 170 ℃ after which the synthesized zeolites were washed, filtered and freeze-dried overnight. The zeolites were calcined at 500 °C for 5 h (5 °C/min) in air, ion-exchanged twice with 1M ammonium nitrate followed by washing, filtration and freeze-drying overnight. The H^+-form of the zeotype was obtained by calcination at 550 °C for 5 h (4 °C/min) in air. The material properties are summarized in Table 1. Elemental analyses were carried out using X-ray fluorescence (XRF) spectrometry on a Malvern-PANalytical AXIOS instrument. The SiO_2/M_2O_3 ratio (M= Al, Ga) was derived from the elemental composition. Complete XRF analysis can be found in Table 2 in the SI. The crystallinity was analyzed with powder X-ray diffraction (XRD) on a Bruker AXS D8 Discover diffractometer with monochromatic Cu-Kα radiation (0.15406 nm) scanning from 5 to 50° 2θ (acquisition time = 2s, increment = 0.01) Thermogravimetric analysis (TGA) was carried out on a Mettler Toledo TGA/DSC 3+ STARe system over a range of 30 °C to 900 °C (10 °C/min) in 60 ml/min air flow. N_2-physisorption isotherms were measured at 77K using a Micromeritics Tristar 3000 instrument after drying the samples at 250 °C for ≥ 16 h in N_2-flow. Acid sites were determined by temperature-programmed desorption of ammonia (NH_3-TPD) as described below. Morphological analysis was carried out using Scanning Electron Microscopy (SEM) on a Zeiss Ultra 55 FEG scanning electron microscope. An accelerating voltage of 1.5 kV was used and backscattered electrons were measured using an SE2 detector. Additional in-depth characterization of the materials is available elsewhere for Silicalite-1 [26] and Ga-silicate [21, 24].

Table 1 Physico-chemical properties of the catalytic materials. M=Al, Ga

Sample	Si/Al	M/ wt%	SA[a]/ $m^2\ g^{-1}$	S^b_{micro}/ $m^2\ g^{-1}$	S^b_{ext}/ $m^2\ g^{-1}$	V^b_{micro}/ $cm^3\ g^{-1}$	Acidity[c]/ mmol g^{-1}
Silicalite-1	–	0	395	386	9.3	0.175	0.002 ± 0.000
Ga-Silicate	33	3.23	365	338	27.3	0.145	0.174 ± 0.005
H-ZSM-5(41)	41	1.04	390	374	15.9	0.164	0.175 ± 0.002
H-ZSM-5(11)	11	3.49	412	386	26.4	0.158	0.582 ± 0.043

[a] apparent surface area by BET method, p/p_0 = 0.002-0.03 for Si-1 and p/p_0 = 0.002-0.05 for H-ZSM-5 and Ga-silicate following consistency criteria [27]

[b] by t-plot method (Harkins and Jura equation, t = 5.0-8.0 Å).

[c] Average of two subsequent NH_3-TPDs

2.2 Flow Reactor Setup and On-line Analytical Instrumentation

A chemical flow reactor was used to evaluate the catalytic properties of the samples and to characterize their acidity. The reactor consisted of a quartz glass tube (ID = 4 mm) surrounded by a metal coil and insulation for resistive heating, see Fig. S1 in the supplementary information (SI). A K-type thermocouple was inserted in the catalyst bed to measure the catalyst temperature and another one was placed in front of the catalyst and used for controlling the inlet gas temperature with a PID regulator (Eurotherm, Worthing, UK). For the catalytic tests in the chemical flow reactor, the catalyst materials were pressed into pellets (5 bar), ground, and sieved to a particle size of 300 µm to 350 µm to avoid detrimental pressure drop. The catalyst sample (ca. 65 mg) was held in place by plugs made of quartz wool (Sigma Aldrich) on each side. Feed gas mixtures of O_2 and Ar were introduced via mass flow controllers (Bronkhorst Hi-Tech, Low-ΔP-flow). The liquid reactant 2,5-dmf was introduced via a gas saturator with argon as a carrier gas. The total flow in the reactor was 300 mL_n/min. The reactor outlet was directly connected via heated Swagelok connections to the analytical instrumentation, consisting of an ion-molecule-reaction mass spectrometer (IMR-MS, Airsense Compact, V &F) and an FTIR gas analyzer (MKS MultiGas 2030). The gas composition was monitored and the reaction products were quantified according to a previously described method combining mass spectrometry and FTIR spectroscopy [22] Some adjustments and additions to the analysis bands were necessary to quantify ammonia in the gas stream. Details of the IR-bands are shown in Table S1 in the SI. IR spectra were recorded every 3.75 s or 15 s between 4000 cm^{-1} to 600 cm^{-1} with a resolution of 0.5 cm^{-1}. Spectra collection and analysis were carried out with the MKS software suite MG2000 v.10.2. and FTIR-library v.R3 supplemented with in-house calibrations described elsewhere [22] A background spectrum in Ar was taken at the beginning of each experiment; IR cell temperature is 191° C.

2.3 Catalytic Tests

Before each experiment, the catalyst was pretreated in 20% O_2 during a temperature ramp of 20° C min^{-1} from room temperature up to 630° C at which it was dwelled for at least 30 min as to remove coke depositions and/or adsorbed species. 2,5-dmf (liquid, Apollo scientific 99% or Sigma-Aldrich ≥ 99%), ethene (4% in Ar) and NH_3 (4% in Ar) were used as feedstocks. Catalytic tests were performed as step response experiments, in which the catalyst was continuously exposed to reactants, i.e., 2,5-dmf, ethene, or a mixture of both at a steady temperature (typically 400 ° C, 450 ° C and 500 ° C).

2.4 Ammonia-TPD

Temperature programmed desorption of NH_3 was carried out in the above-described reactor to determine the total amount of acid sites of the catalysts. The catalyst samples were exposed to two 30 min pulses of 280 ppm NH_3 to ensure full adsorption at 100 ° C. Then the samples were purged with pure Ar for 90 min followed by a temperature ramp of 10 ° C min^{-1} from 100 ° C to 600 ° C to desorb NH_3. The amount of acid sites of the fresh samples (before the catalytic tests) is determined by the detection of desorbed ammonia during the temperature ramp assuming that an acid site adsorbs one ammonia molecule [28]. The TPD profile is analyzed by applying a baseline correction and deconvolution using symmetric gaussian functions. In the same way, the amount of acid sites after the catalytic tests (without oxidative regeneration of the catalyst) is determined. The difference indicates how many and which types of acid sites are deactivated due to coking.

3 Results and Discussion

We start off this section by commenting on the characteristics of the catalysts. Then follows a discussion of the catalytic performance tests utilizing bio-derived 2,5-dmf and a comparison of H-form Ga-silicate, commercial H-ZSM-5(11), synthesized H-ZSM-5(41), and Silicalite-1. We discuss how the gallium modification affects product distribution and selectivities, overall aromatics production as well as long-term stability and deactivation of the catalyst. Some focus is put on acid site characterization, especially by NH_3 -TPD measurements, before and after the catalytic performance tests. Finally, we discuss how co-feeding ethene affects aromatics production.

3.1 Catalyst Characterization

XRD X-ray diffraction was measured for Silicalite-1, Ga-silicate, and the two ZSM-5 catalysts, and the corresponding normalized patterns are shown in Fig. S2 in SI. All four samples exhibit diffraction peaks around $2\theta = 8.00°$, 8.87°, 9.14°, 14.0°, 14.8°, 23.1°, 23.4°, 24.0°, 24.4°, 29.9°, corresponding to the (101), (200), (111), (012), (031), (051), (501), (033), ($\bar{3}$13)and (053) planes respectively. These are characteristic of the MFI framework structure [29] and the absence of other peaks indicates that no additional crystalline phases with long-range order are formed. Slight differences in relative peak intensities can be caused by the distortion of the unit cell caused by aluminium and gallium substitution, by the different synthesis methods of

commercial H-ZSM-5 and the synthesized materials, or by different measurement settings such as a small sample slit size, which increases the intensity at low 2θ values.

XRF The chemical composition of the samples was determined by XRF (Table S2 in SI). The normalized aluminium content of the commercial ZSM-5 sample was determined to be 3.5 wt% which amounts to a ratio of Si/Al=11. The gallium content of Ga-silicate is 3.2 wt% which amounts to a ratio of Si/Ga=33. In order to compare the influence of the substituted metal in a meaningful way, an H-ZSM-5 sample of a comparable Si/Al ratio was synthesized. Its aluminium content was determined to be 1.0 wt% which amounts to a ratio of Si/Al=41. Silicalite-1 did not contain any aluminium or gallium but for all three samples, some traces of other elements, such as sodium, were measured at a ppm level. These impurities most likely originate from the precursor material sodium hydroxide.

SEM SEM images in Fig. S3 in SI show the morphological features of the synthesized materials and confirm crystallinity. Silicalite-1 crystals and ZSM-5(41) crystals are coffin-shaped whereas ZSM-5(11) contains both coffin-shaped and cubic-shaped crystals. Ga-silicate crystals are cubic-shaped and have formed larger, connected intergrowths, suggesting the presence of mesopores [24]. In all samples, irregular structures were identified on the external facets, suggesting the presence of impurities or the potential migration of Al or Ga species during calcination [24]. In previous work, it was concluded that Ga was still inside the framework of Ga-silicate using diffuse reflectance infrared Fourier transform spectroscopy (DRIFTS) [24]. The vibration at 3616 cm^{-1} confirms the presence of Brønsted acid sites caused by the OH stretch vibration in the -Ga-O(H)-Si- species. Compared to Al-silicate (ZSM-5) the vibration is shifted from 3610 cm^{-1} to higher wavenumbers confirming the weaker Brønsted acid strength of the Ga sample [21, 26].

TGA TGA was carried out and the weight loss profiles are shown in Fig. S4 in SI. The total weight losses of 1.2%, 3.3%, 4.0 % and 8.7% for Silicalite-1, Ga-silicate, ZSM-5(41), and ZSM-5(11) respectively, indicate high thermal stability for all samples over this temperature range. Most of the weight loss occurred between 50 ° C and 200° C, indicating the loss of water adsorbed from the air [30].

N_2-sorption. N_2-isotherms are shown in Fig. S5 in SI. Isotherms of ZSM-5(11), Silicalite-1 and Ga-silicate are classified as Type IV isotherms, typical for porous materials containing both micropores and mesopores, further confirming crystal agglomerates of the MFI structure [31]. ZSM-5(41) has a Type I isotherm which is typical for microporous materials with a broader range of micropores and possibly small mesopores. However, an increase in nitrogen adsorption at high relative pressure suggests that if more points were collected at higher relative pressure, a Type IV isotherm could be identified. For Silicalite-1, capillary condensation occurs at $p/p_0 = 0.15$, demonstrated by a step in nitrogen adsorption, and at $p/p_0 = 0.4$, indicated by hysteresis loops at both relative pressures. For ZSM-5(11) and Ga-silicate, capillary condensation occurs at $p/p_0 = 0.4$, indicated by hysteresis loops. Type H4 hysteresis loops present in these three samples indicate the presence of both micro- and mesopores [31]. Type H1 hysteresis found at $p/p_0 = 0.15$ in Silicalite-1 suggests the presence of well-defined channels with uniform sizes and shapes [32]. The absence of a hysteresis in ZSM-5(41) supports its Type I isotherm and indicates the presence of small micropores.

NH_3 -TPD and acid sites. The total acidity was determined by NH_3-TPD in the same reactor setup as the catalytic performance tests and with the same samples. NH_3 -TPD is a technique that can easily be applied to acid catalysts to determine the total amount of acid sites because the ammonia molecule interacts with the acid sites. However, this technique only provides an effective strength because the ammonia molecule can readsorb, which is dependent on experimental parameters, such as flow rate and diffusion [33]. Nevertheless, the apparent strength of different acid sites can be observed and distinguished from the desorption profile. To discriminate between Brønsted and Lewis acid types, other probe molecules such as pyridine are often used in combination with *in situ* IR spectroscopy [34].

Typically, when probing the acid sites of zeolite materials with NH_3, at least two main peaks are detected, which can be referred to as a low-temperature and a high-temperature peak. The former is attributed to weakly bound ammonia, which can be removed by a long purge time, evacuation, or treatment with water vapor [35, 36]. However, the high-temperature peak is not affected by such treatments and is often considered to be related to the relevant catalytic centers. The results of the NH_3-TPD are only discussed briefly here, and in more detail in a later section. The total densities of acid sites for the catalysts are shown in Table 1. As expected, Silicalite-1 contains almost no acid sites with a density of 0.002 mmol g^{-1}. These sites are very weak and are attributed to silanol groups with desorption peaks at 133 ° C and 159 ° C. In contrast, ZSM-5(11) has a relatively high acid site density of 0.582 ± 0.043mmol g^{-1} which is because of its high aluminium content. The relation between the aluminium content and the acid site density is confirmed by the synthesized ZSM-5(41), which has a much lower acid site density of 0.175 ± 0.002 mmol g^{-1}. Ga-silicate has a very similar acid site density of 0.174 ± 0.005 mmol g^{-1}, which allows for relating catalytic activity to the nature of the acid sites, as opposed to the amount. The fact that Ga-silicate has a similar acid site density as ZSM-5(41) while it has a higher metal loading, could be caused by framework Ga species that migrated to the external facets during calcination. The NH_3-TPD profile shows a shoulder at relatively high temperatures of 436 ° C and 493 ° C which has been

assigned to extra framework Gallium species [36]. Considering this, both ZSM-5 samples show a shoulder at a relatively higher temperature of 383 ° C (11) and 469 ° C(41), indicating some extra-framework Al species.

In summary, all samples are characterized as microporous materials of the MFI framework. The amount of acid sites is as expected very low for the silicalite-1 and relatively high for ZSM-5(11). ZSM-5(41) and Ga-silicate have similar acid site densities and the results indicate the presence of extra-framework Ga species, even though Ga is still present in the framework. Both ZSM-5(11) and Ga-silicate show some mesoporosity.

3.2 Selectivity Shifts from Aromatics to Isomers

In the continuous step response catalytic performance tests, Ga-silicate was exposed to a vapor of 2,5-dmf in Ar at 500 ° C as shown in Fig. 1. Initially, all 2,5-dmf is converted mainly to benzene and to a lesser extent to other aromatics, such as toluene, xylenes, and indene, as well as to olefins such as propene, ethene, and butadiene. Both propene and toluene show production maxima after about 20 min time-on-stream (TOS), which is later than that for benzene. Clearly, the formation of aromatics and olefins is decreasing gradually. After a while, the formation of 2,4-dimethylfuran (2,4-dmf), 2-methyl-2-cyclopentenone (2-mcpo), and 3-methyl-2-cyclopentenone (3-mcpo) begins and increases with TOS until the end of the three-hour experiment. These three compounds all represent structural isomers of the reactant 2,5-dmf. A similar selectivity shift from olefins and aromatics with increasing TOS has been reported previously for H-ZSM-5, Cu-ZSM-5, and beta zeolites [23]. The change in selectivity has been proposed to be related to the characteristics of the available acid sites as is further discussed below.

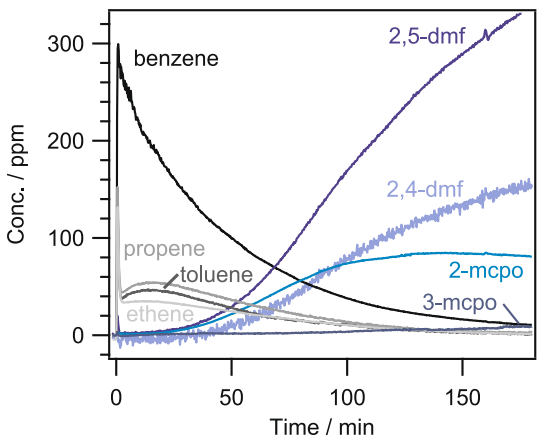

Fig. 1 Concentration profiles of benzene, propene, toluene, ethene, 2,5-dmf, 2,4-dmf, 2-mcpo, and 3-mcpo during a 90-minute step response experiment. Feed: 800 ppm 2,5-dimethylfuran, 500 ° C, catalyst: 68.8 mg Ga-silicate

Some of the acid sites are deactivated due to coking, which is visually evident from the black coloring of the catalyst and supported by the formation and release of carbon oxides when the catalyst is regenerated in oxygen.

3.3 Influence of Co-feeding Ethene

It has been reported that co-feeding ethene or propene with furans can enhance aromatics production [7]. A diene such as ethene and a dienophile such as 2,5-dmf could form the highly desired *p*-xylene product via cycloaddition (Diels-Alder reaction) and subsequent dehydration. Co-feeding ethene should thus increase the selectivity to *p*-xylene if the reaction occurs via a cycloaddition and dehydration mechanism under these conditions. In a 60 min step response experiment, 2,5-dmf and ethene (ratio ca. 1:1) were co-fed to a Ga-silicate catalyst at 400 ° C. This experiment was repeated without any additional ethene under otherwise the same conditions. As can be seen in Figs. 2 and S6 in the SI, the BTX products are not affected by the additional ethene. At best, minor increases in propene and toluene formation are detected when there is no additional ethene. However, there is no difference in xylene formation. Further experiments (not shown) at 300 and 500 ° C lead to the same conclusion, while the formation of xylenes at these temperatures

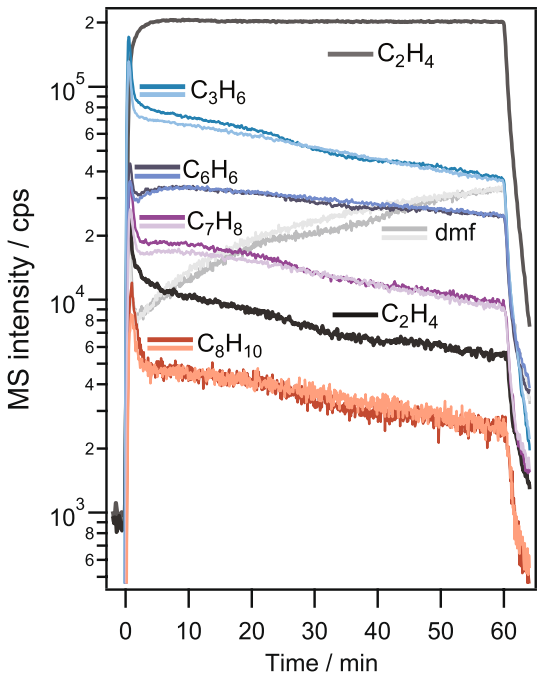

Fig. 2 MS intensity profiles of ethene (C_2H_4, dark gray), propene (C_3H_6, light blue), benzene (C_6H_6, dark blue), toluene (C_7H_8, purple), dimethylfuran (light gray) and xylenes (C_8H_{10}, red) during 60-min step response experiments, once without (dark color) and once with (light color) additional ethene feed (730 ppm). Feed: 800 ppm 2,5-dmf, 400 ° C, catalyst: 68.8 mg Ga-silicate

is lower than at 400 ° C. Feeding only ethene to the Ga-silicate catalyst results in the detection of small amounts of propene, benzene, and toluene, but no xylenes (see Fig. S7 in SI). This is another indicator that the slightly higher amounts of propene and toluene detected during co-feeding ethene and 2,5-dmf are independent, meaning no cycloaddition reactions are happening. When comparing the formation of aromatics at different temperatures, the formation of toluene and xylenes is generally favored at around 450 ° C whereas at higher temperatures, the selectivity shifts further to benzene, which is comparable to studies with other zeolites [23]. Hence, one can conclude that under the studied reaction conditions, the formation of BTX aromatics is unlikely to involve cycloaddition reactions to any significant extent. Instead, aromatization must originate from the hydrocarbon pool, mainly consisting of olefinic species. These olefins and their carbocations are formed through cracking, decarbonylation and dehydration reactions and are then subject to acid catalyzed oligomerization and aromatization resulting in BTX, but also heavier polycyclic aromatics such as (substituted) indenes and naphthalenes, which are likely precursors of deactivating coke [37]. A reaction scheme illustrating these pathways is shown in Fig. 6.

3.4 Long-Term BTX Production

The Ga-silicalite and ZSM-5 catalysts were evaluated in longer experiments lasting 10 h. Silicalite-1 was tested as well but did not show any conversion of 2,5-dmf (see Fig. S8 in SI), because of the lack of acid sites, and will therefore not be discussed further. In Fig. 3, the signals for BTX aromatics measured by an IMR-MS (Hg, ionizing potential 10.44 eV) at m/z = 78, 92, and 106 are shown. The BTX signals for Ga-silicate are compared to the ones for ZSM-5. There is a distinct difference in the BTX profiles: The ZSM-5(11) sample shows an initial high formation of BTX with a relatively fast decrease and complete stop of production (toluene, xylene), whereas the Ga-silicate sample shows an initial high benzene production which gradually decreases over the course of the 10 h experiment. Comparing Ga-silicate to a catalyst with similar acid site density, ZSM-5(41), further illustrates the former's high selectivity to benzene and slower deactivation. The total amount of detected BTX molecules after 10 h reaction at 500 ° C is summarized in Table 2 and visualized in Fig. S9 in SI, normalized to the amount of catalyst and acid sites. Here it can be seen that the Ga-silicate and ZSM-5 catalysts produce similar amounts of toluene and xylene. However, the amount of benzene produced by Ga-silicate is more than twice or eight times as much as ZSM-5(11) and ZSM-5(41) respectively, mainly attributed to slower deactivation. This could be attributed to the nature of the acid sites since Ga-silicate and ZSM-5(41) have the same acid site density.

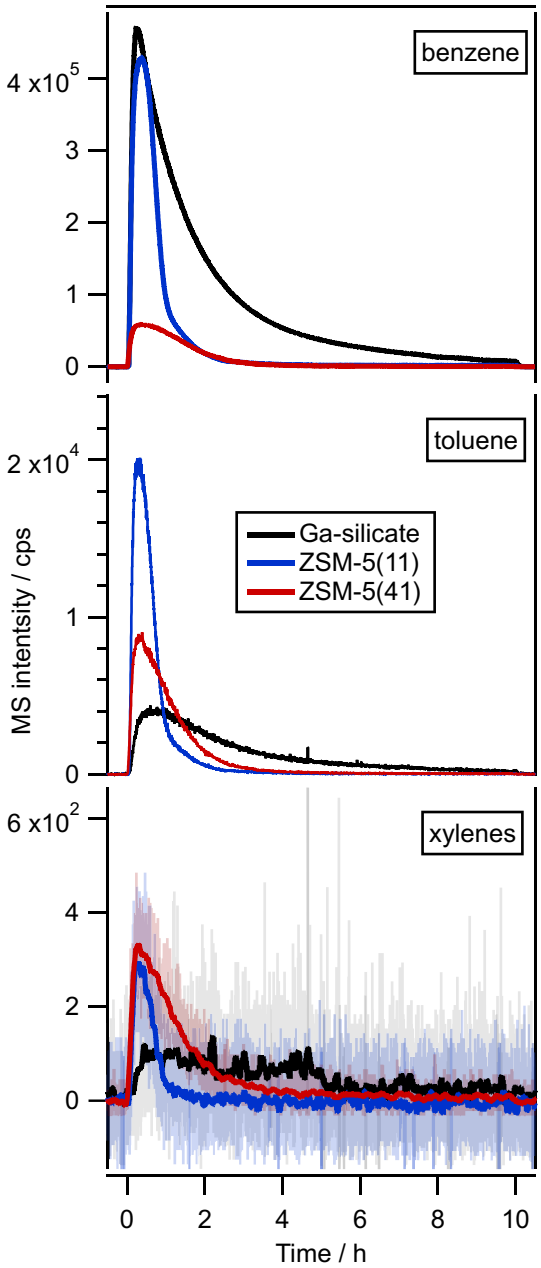

Fig. 3 MS intensity signals of benzene, toluene, and xylenes (includes the averaged signal) during a 10 h catalytic experiment for Ga-silicate (black), ZSM-5(11) (blue) and ZSM5(41) (red) samples. Conditions: after pretreatment in 20% O_2 at 550 ° C and NH_3-TPD. Feed: 540 ppm 2,5-dimethylfuran, 500 ° C, catalyst: 77.5 mg Ga-silicate, 65.6 mg ZSM-5(11) and 76.0 mg ZSM-5(41)

In Fig. 4, the conversion and selectivities for aromatics, olefins, and isomers of 2,5-dmf are shown. The selectivities shown include no carbon loss due to coking because the amount of coke deposition on the catalyst surface

Table 2 BTX production for catalyst samples Ga-silicate and ZSM-5, detected by MS (counts) and normalized to the amount of catalyst and acid sites

Sample	Ga-silicate 10^6 counts/g	ZSM-5(11)	ZSM-5(41)	Ga-silicate 10^6 counts/ acid site	ZSM-5(11)	ZSM-5(41)
Benzene	41,094	19,587	4887	229,578	36,408	28,251
Toluene	589	760	531	3288	1412	3071
Xylenes	24	9	26	132	17	148
Total	41,707	20,356	5444	232,998	37,836	31,470

cannot be tracked in real-time. The carbon selectivity of coke is typically found to be between 16 and 20%. Thus, taking into account coking, the selectivities in Fig. 4 would become somewhat lower. Over the entire test period of 10 h, about 90% of the carbon is detected and quantified using FTIR including the formed coke, which is released mostly as CO and CO_2 during a temperature-programmed oxidation (TPO) and regeneration of the catalyst. This amounts to a carbon balance of 90% with 10% unidentified species [22]. The graphs display a slower decrease in conversion and aromatics production for the Ga-silicate sample. It also shows higher selectivity to benzene, but lower selectivity to toluene. Remarkably, after the initial formation of aromatics and olefins, the selectivity shifts to 2,4-dmf, 2-mcpo, and 3-mcpo, which are all isomers of the reactant 2,5-dmf. Their production is still notable after 10 h of TOS. In contrast, the ZSM-5(11) sample is nearly completely inactive after 3h of TOS and the ZSM-5(41) remains selective to 2,4-dmf after 10 h. Noteworthy, the ZSM-5(11) sample could not be completely regenerated in 20% oxygen in the reactor, as some coke depositions remained on the catalyst even at 630 ° C as indicated by visible black catalyst particles and the same conversion could not be achieved again. To investigate the stability of Ga-silicate, the catalyst was subjected to four more catalytic cycles of 2,5-dmf conversion (2 h each) at 500 ° C, separated by an oxidizing regeneration step of 1 h at 608 ° C in 20% O_2, shown in Fig. S10 in the SI. During the four cycles, the conversion after 2 h decreased from 43% in cycle one to 39 % in cycle four whereas the initial benzene selectivity decreased from 63 % in cycle one to 59 % in cycle four. Moreover, the product distribution and selectivities remained similar. Thus one can conclude that the Ga-silicate is readily generated and remains active after several cycles of 2,5-dmf conversion.

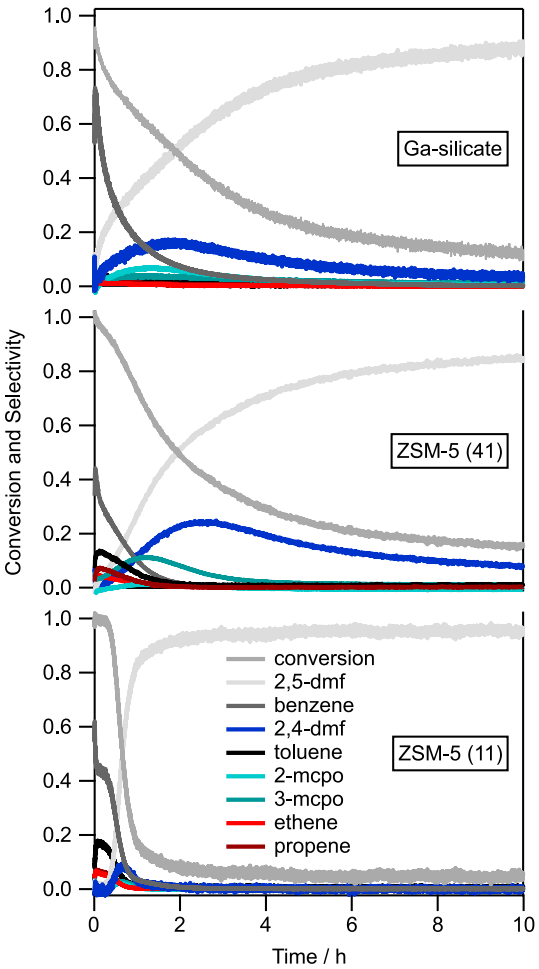

Fig. 4 Conversion and selectivity of 2,5-dmf, benzene, toluene, ethene, propene, 2,4-dmf, 3-mcpo, and 2-mcpo during a 10 h step response experiment. Note: the shown selectivities do not account for the carbon loss due to coking. Feed: 540 ppm 2,5-dimethylfuran, 500 ° C, catalyst: 77.5 mg Ga-silicate (top panel), 76.0 mg ZSM-5(41) (middle panel) 65.6 mg ZSM-5(11) (bottom panel)

3.5 Change of Acid Site Availability

The different results for ZSM-5 and Ga-silicate sparked interest in how the acid sites differ and what causes the suppressed deactivation of Ga-silicate. The NH_3-TPD profiles can be analyzed by deconvolution and distinguishing various acid sites by their strength. Previously, four different peaks of different acid strengths have been identified for H-ZSM-5 catalysts and other metal oxides [38]. In this work, we have grouped the analyzed peaks by their temperature of maximum desorption into weak (w, ≤ 200° C), medium (m, 200 ° C to 250 ° C), strong (s, 250 ° C to 350 ° C) and extra-framework (ex, ≥ 350° C) acid sites. The results for the two catalysts are summarized in Table 3 and Fig. 5 before and

Table 3 Analysis of the NH_3 -TPD profiles right before and after the reaction. Desorption peaks are grouped into weak (w, ≤ 200° C), medium (m, 200 ° C and 250 ° C), strong (s, 250 ° C and 350° C) and extra-framework (ex, ≥ 350° C) acid sites

Sample		Ga-silicate			ZSM-5(41)			ZSM-5(11)		
Status	Peak #	T /° C	C / mmol g^{-1}		T /° C	C / mmol g^{-1}		T /° C	C / mmol g^{-1}	
Fresh	1	174	0.028	w	175	0.022	w	177	0.139	w
	2	301	0.136	s	300	0.087	s	227	0.107	m
	3	436	0.008	ex	349	0.059	s	319	0.285	s
	4	493	0.008	ex	472	0.005	ex	382	0.007	ex
	Total		0.179			0.173			0.538	
Spent	1	170	0.006	w	161	0.005	w	171	0.081	w
	2	216	0.008	m	198	0.007	w	235	0.119	m
	3	283	0.014	s	300	0.021	s	332	0.160	s
	Total		0.029			0.033			0.359	

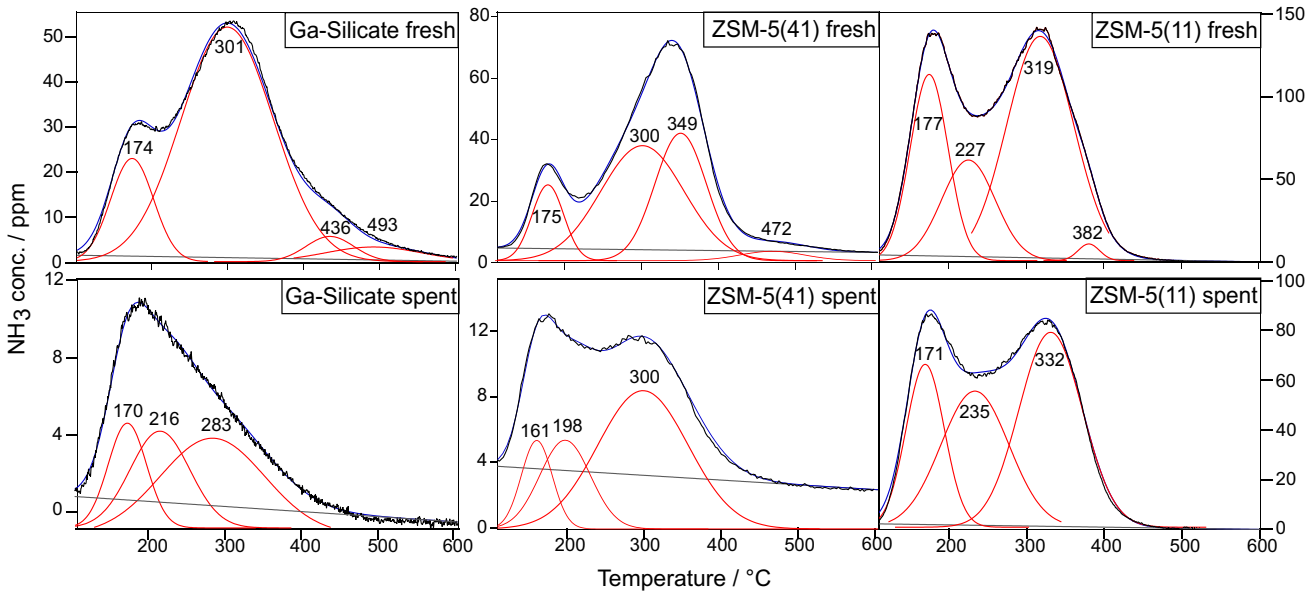

Fig. 5 Analysis of the ammonia TPD profiles measured directly before (top panels: fresh catalyst) and after (bottom panels: spent catalyst) the 10 h catalytic conversion experiment with 2,5-dmf. Measured ammonia (black), fitted curve (blue), background (gray), and deconvoluted peaks (red). NH_3-adsorption: 30 min 280 ppm NH_3, 90 min Ar purge, NH_3-TPD: temperature ramp 10 ° C min^{-1}

after a 10 h 2,5-dmf conversion experiment. The available acid site density for the Ga-silicate sample has decreased from 0.179 to 0.029 mmol g^{-1}, which is a decrease of 0.150 mmol g^{-1} or 84%. It is worth mentioning, that at this point the sample is still active for converting 2,5-dmf. In contrast, the ZSM-5(11) sample which has a much higher initial acid site density, decreased from 0.538 to 0.359 mmol g^{-1} or by 33%. However, at this point, the ZSM-5(11) catalyst is not active anymore. ZSM-5(41), which has an initial acid site density similar to Ga-silicate of 0.173 mmol g^{-1}, shows a decrease of 81% with 0.033 mmol g^{-1} available acid sites after the conversion experiment and also remained active to converting 2,5-dmf.

The desorption peaks at the respective highest temperatures of 436 ° C and 493 ° C for Ga-silicate, 472 ° C for ZSM-5(41) and 382 ° C for ZSM-5(11) were attributed to extra-framework sites. In another work, it was suggested that the extra-framework gallium is located in the ion-exchange site and synergistically interacts with framework gallium to form a strong acid site [36]. Pyridine adsorption IR determined that the site was a Lewis acid site. This peak was not observed when gallium was impregnated into silicalite-1, indicating that the strong Lewis acid sites only form in the presence of Brønsted acid sites [39]. It was suggested that if heteroatoms such as Ga could be placed selectively in specific T sites, this would open the opportunity to direct the spatial distribution of Lewis acid sites for bifunctional catalysts, which might be of advantage for aromatics production [40]. However, one should be careful when assigning Lewis acidity to extra-framework species since another work has established that the amount of extra-framework aluminium is not always correlating with the total number of Lewis sites

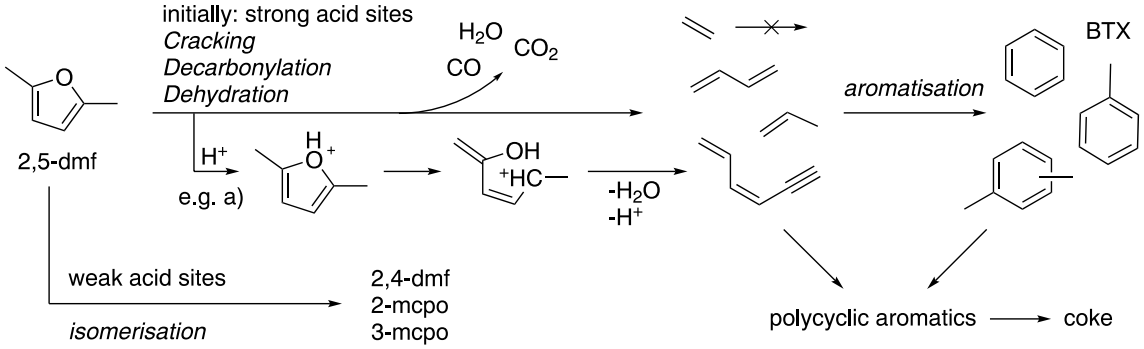

Fig. 6 Proposed reaction scheme for the catalytic conversion of 2,5-dmf. Initially available strong acid sites are mainly responsible for providing the olefinic hydrocarbon pool through cracking, decarbonylation, and dehydration of the reagent. A possible pathway a) was suggested by Uslamin et al [43]. Subsequent aromatization leads to BTX. Weak acid sites remain active for isomerization reactions to 2,4-dmf, 2-mcpo, and 3-mcpo

in several zeolites [17]. For all three catalysts, the extra-framework sites disappeared after the 10 h step response experiment. It seems likely that this disappearance can be attributed to the coking of the catalyst surface, deactivating the extra-framework sites. The disappearance also indicates that extra-framework sites can at least not be responsible for isomerization reactions leading to the formation of e.g., 2,4-dmf. Hence, we can assume that isomerization reactions occur over weak acid sites inside the micropores. The extra-framework sites could on the other hand be responsible for cracking reactions resulting in olefinic intermediates, in this way providing the feedstock for aromatics formation. This unsaturated olefinic hydrocarbon pool is then subject to acid catalyzed aromatization. It has been suggested that well-dispersed Ga^{3+}+ species, such as $[GaH_2]^+$ are responsible for increasing BTX selectivity (in contrast to inactive Ga_2O_3 species) [40].

The strong peaks at 301 ° C for Ga-silicate, 300 ° C and 349 ° C for ZSM-5(41) and 319 ° C for ZSM-5(11), associated with Brønsted acid sites [41], significantly decrease for all samples, suggesting that they play a role in BTX formation. These findings might support previous studies that suggest the interplay of Lewis acidic extra-framework sites with BAS for increased aromatization [40].

The small number of weak acid sites in the Silicalite-1 sample did not show any 2,5-dmf conversion. We can thus assume that catalytic activity for this reaction towards BTX is mainly caused by medium, strong and extra-framework acid sites. Even though some medium and strong acid sites are detected by NH_3-TPD after the 10 h experiment, not all of them are still active. There can be several reasons for this: (1) some of these acid sites are only accessible to the small NH_3 molecule, but not to the bigger 2,5-dmf molecule after the buildup of coke that blocks accessibility to acid sites. (2) some of these acid sites are still accessible to 2,5-dmf but are only resulting in the isomerization of 2,5-dmf as for the Ga-silicate sample. (3) NH_3 interacts with coke in a similar way as with acid sites. Such interaction resulting in an almost identical desorption profile is however unlikely. The effect of coke is mainly to reduce the number of available acid sites without measurable change in strength and distribution [42]. Furthermore, no reaction products between NH_3 and coke could be detected during the NH_3-TPD. Some CO and CO_2 is only released—due to the high temperature—after almost all NH_3 had already desorbed.

To summarize this section, we can suggest that initially available strong acid sites, consisting of both strong Brønsted and Lewis acid sites are responsible in providing the unsaturated olefinic hydrocarbon pool through decarbonylation, dehydration, and cracking of the reactant 2,5-dmf. One such pathway is suggested in another work [43] as shown in the reaction scheme in Fig. 6. The olefin pool (except for ethene under the reaction conditions studied here) is then subject to oligomerization and aromatization, for which the presence of Ga species seems beneficial. The strong acid sites are rapidly deactivated. However, some of them remain accessible to detection by NH_3-TPD, suggesting that not all strong acid sites are relevant for aromatization.

Weak acid sites on the other hand are suggested to remain active much longer for isomerization reactions, such as acid catalyzed methyl-shift resulting in 2,4-dmf and ring opening and rearrangement reactions resulting in 2-mcpo and 3-mcpo.

TPO The release of CO and CO_2 during the TPO of the coke depositions also indicates differences between Ga-silicate and ZSM-5(11). During the 10 h experiment, the Ga-silicate sample accumulated 7.7 wt% of coke (measured as C1, not considering hydrogens) whereas the ZSM-5(11) sample accumulated 6.7 wt% (Silicalite-1 did not accumulate any significant amount of coke). The Ga-silicate also released more CO (1.67 $mmol/g_{cat}$) compared to ZSM-5(11) (0.65 $mmol/g_{cat}$) but less CO_2 (3.14 $mmol/g_{cat}$ vs 4.08

mmol/g_{cat}) during the TPO. Finally, the peak maxima for the CO and CO_2 release for the Ga-silicate sample are lower than the ZSM-5(11) sample (559 and 553 vs 587 and 578 ° C respectively). The coke that is formed must thus be different, i.e. in composition, or where it forms. This leads to the blocking of different active sites and distinct selectivities and deactivation behavior. The effect of the heteroatom in the framework structure obviously plays a significant role in the selectivity and deactivation behavior of the catalyst. It needs to be discussed what exactly this effect is. Acidic sites created by Ga-atoms should have a different acid strength than those created by Al-atoms. Brønsted acid sites (BAS) in Ga-silicate are weaker than those in Al-silicate. Previous studies have shown, that this difference is however rather small. The acid site strength (MFI ca. 130kJ mol^{-1}) was found to be similar to the acid sites in ZSM-5 [36, 44, 45] and different framework structures were found to have a bigger effect than the composition [36]. Strong Lewis acid sites from extra-framework Ga paired with framework Ga-sites were found to favor aromatization [40]. Another factor that could be a reason for the observed catalytic differences is the size of the heteroatom. The bigger Ga-atom in the framework results in smaller pore size [20], which could be attributed to greater selectivity towards the smaller aromatics, e.g. benzene, and slower formation of bulky polyaromatics that lead to coking and catalyst deactivation, as observed in this work.

For a deeper understanding, more extensive studies are necessary, for example combining the use of probe molecules of different sizes and adsorption strength (substituted benzenes and pyridines) to distinguish between external and internal acid sites, silanols, and acidic bridging Si–Al–OH or Si–Ga–OH groups with in situ FTIR spectroscopy [46]. Another tool could be 2D MAS NMR spectrometry as it has been studied for the isomerization of xylenes [47].

4 Conclusions

In this work, we evaluated Silicalite-1, Ga-silicate, and two H-ZSM-5 catalysts for the continuous conversion of bio-derived 2,5-dimethylfuran to value-added chemicals, such as BTX, olefins, and isomers of 2,5-dmf. The presence of a heteroatom in the MFI structure seems crucial to creating acid sites and thus catalytically active sites for these reactions since Silicalite-1 itself is completely inactive. The Ga-silicate showed much longer activity compared to the Al-containing isomorph, ZSM-5(11), and an increased benzene selectivity compared to ZSM-5(41). The suppressed deactivation of active sites resulted in a longer and thus higher total production of BTX aromatics compared to both ZSM-5 samples. Co-feeding ethene to promote cycloaddition reactions and hence increase *p*-xylene selectivity did not show the expected effect. We conclude that aromatics formation does not occur through cycloaddition reactions between ethene and 2,5-dmf. Acid site characterization by NH_3-TPD revealed a higher acid site density for the ZSM-5(11) sample compared to the Ga-silicate and ZSM-5(41) samples. After 10 h of catalytic 2,5-dmf conversion, the majority of acid sites of the ZSM-5(11) sample was still detected but the catalyst had become completely inactive for catalytic conversion. Ga-silicate, on the other hand, had lost most of its acid sites, including extra-framework sites, but is still able to convert 2,5-dmf to isomer products, such as 2,4-dmf. In a similar way, ZSM-5(41) lost its strong acid sites and showed high conversion to 2,4-dmf after 10 h while it demonstrated lower initial selectivity to benzene. This implies that for some reactions like isomerization, the acid site density, as well as the acid site strength, are important, while for other reactions like BTX production, the role of the heteroatom and the nature of the acid sites are identified as important factors to steer selectivity and assure long-term activity.

In this case study, Ga-silicate showed enhanced catalytic properties for the valorization of 2,5-dmf. However, further studies are necessary to elucidate the role of the acid site in more detail and understand how the Ga-modification suppresses deactivation of BTX formation functionality.

Supplementary Information The online version contains supplementary material available at https://doi.org/10.1007/s11244-022-01776-2.

Acknowledgements This work is financially supported by the Swedish Research Council for Environment, Agricultural Sciences and Spatial Planning (Formas) [No. 2017-00420] and the Swedish Energy Agency [No. 48569-1].

Funding Open access funding provided by Chalmers University of Technology.

Declarations

Conflict of interest There are no conflicts to declare.

References

1. Ellis LD et al (2021) Chemical and biological catalysis for plastics recycling and upcycling. Nat Catal 4(7):539–556. https://doi.org/10.1038/s41929-021-00648-4

2. Zhu Y, Romain C, Williams CK (2016) Sustainable polymers from renewable resources. Nature 540(7633):354–362. https://doi.org/10.1038/nature21001
3. Ragauskas AJ et al (2006) The path forward for biofuels and biomaterials. Science 311(5760):484–489. https://doi.org/10.1126/SCIENCE.1114736
4. Bosch R, Van De Pol M, Philp J (2015) Policy: define biomass sustainability. Nature 523(7562):526–527. https://doi.org/10.1038/523526a
5. Persha L, Agrawal A, Chhatre A (2011) Social and ecological synergy: local rulemaking, forest livelihoods, and biodiversity conservation. Science 331(6024):1606–1608. https://doi.org/10.1126/SCIENCE.1199343
6. Zhang H, Xiao R, Huang H, Xiao G (2009) Comparison of non-catalytic and catalytic fast pyrolysis of corncob in a fluidized bed reactor. Bioresour Technol 100(3):1428–1434. https://doi.org/10.1016/J.BIORTECH.2008.08.031
7. Cheng YT, Huber GW (2012) Production of targeted aromatics by using Diels-Alder classes of reactions with furans and olefins over ZSM-5. Green Chem 14(11):3114–3125. https://doi.org/10.1039/c2gc35767d
8. Jae J et al (2011) Investigation into the shape selectivity of zeolite catalysts for biomass conversion. J Catal 279(2):257–268. https://doi.org/10.1016/J.JCAT.2011.01.019
9. Luna-Murillo B et al (2021) Catalytic fast pyrolysis of biomass: catalyst characterization reveals the feed-dependent deactivation of a technical ZSM-5-based catalyst. ACS Sustain Chem Eng 9(1):291–304. https://doi.org/10.1021/acssuschemeng.0c07153
10. Coqueblin H et al (2017) Effect of the metal promoter on the performances of H-ZSM5 in ethylene aromatization. Catal Today 289:62–69. https://doi.org/10.1016/J.CATTOD.2016.08.006
11. Espindola JS, Gilbert CJ, Perez-Lopez OW, Trierweiler JO, Huber GW (2020) Conversion of furan over gallium and zinc promoted ZSM-5: the effect of metal and acid sites. Fuel Process Technol 201:106319. https://doi.org/10.1016/j.fuproc.2019.106319
12. Lok CM, Van Doorn J, Aranda Almansa G (2019) Promoted ZSM-5 catalysts for the production of bio-aromatics, a review. Renew Sustain Energy Rev 113:109248. https://doi.org/10.1016/J.RSER.2019.109248
13. Uslamin EA et al (2019) Gallium-promoted HZSM-5 zeolites as efficient catalysts for the aromatization of biomass-derived furans. Chem Eng Sci 198:305–316. https://linkinghub.elsevier.com/retrieve/pii/S0009250918306729. https://doi.org/10.1016/j.ces.2018.09.023
14. Hoff TC et al (2017) Elucidating the effect of desilication on aluminum-rich ZSM-5 zeolite and its consequences on biomass catalytic fast pyrolysis. Appl Catal A 529:68–78. https://doi.org/10.1016/J.APCATA.2016.10.009
15. Cheng YT, Jae J, Shi J, Fan W, Huber GW (2012) Production of renewable aromatic compounds by catalytic fast pyrolysis of lignocellulosic biomass with bifunctional Ga/ZSM-5 catalysts. Angew Chem Int Ed 51(6):1387–1390. https://doi.org/10.1002/ANIE.201107390
16. Zheng Y et al (2017) Study on aromatics production via the catalytic pyrolysis vapor upgrading of biomass using metal-loaded modified H-ZSM-5. J Anal Appl Pyrol 126:169–179. https://doi.org/10.1016/J.JAAP.2017.06.011
17. Ravi M, Sushkevich VL, van Bokhoven JA (2020) Towards a better understanding of Lewis acidic aluminium in zeolites. Nat Mater 19(10):1047–1056. https://doi.org/10.1038/s41563-020-0751-3
18. Fang Y et al (2017) Aromatization over nanosized Ga-containing ZSM-5 zeolites prepared by different methods: effect of acidity of active Ga species on the catalytic performance. J Energy Chem 26(4):768–775. https://doi.org/10.1016/J.JECHEM.2017.03.014
19. Li J et al (2015) Maximizing carbon efficiency of petrochemical production from catalytic co-pyrolysis of biomass and plastics using gallium-containing MFI zeolites. Appl Catal B 172–173:154–164. https://doi.org/10.1016/J.APCATB.2015.02.015
20. Li J, Li X, Hua D, Lu X, Wang Y (2019) Optimizing the aromatic product distribution from catalytic fast pyrolysis of biomass using hydrothermally synthesized Ga-MFI zeolites. Catalysts 9(10):854. https://doi.org/10.3390/catal9100854
21. Creci S (2020) Tuned acidity in zeotypes: a descriptor to unravel the direct conversion of methane to methanol. Ph.D. thesis, Chalmers University of Technology, Gothenburg. https://research.chalmers.se/en/publication/520850
22. Sauer C, Lorén A, Schaefer A, Carlsson P-A (2021) On-line composition analysis of complex hydrocarbon streams by time-resolved Fourier transform infrared spectroscopy and ion-molecule reaction mass spectrometry. Anal Chem 93(39):13187–13195. https://doi.org/10.1021/ACS.ANALCHEM.1C01929
23. Sauer C, Lorén A, Schaefer A, Carlsson A (2022) Valorisation of 2,5-dimethylfuran over zeolite catalysts studied by on-line FTIR-MS gas phase analysis. Catal Sci Technol 12(3):750–761. https://doi.org/10.1039/D1CY01312B
24. Creci S, Martinelli A, Vavra S, Carlsson PA, Skoglundh M (2021) Acidity as descriptor for methanol desorption in B-, Ga- and Ti-MFI zeotypes. Catalysts 11(1):97
25. Szostak R, Nair V, Thomas TL (1987) Incorporation and stability of iron in molecular-sieve structures. Ferrisilicate analogues of zeolite ZSM-5. J Chem Soc Faraday Trans 83(2):487–494
26. Creci S, Wang X, Carlsson PA, Skoglundh M (2019) Tuned acidity for catalytic reactions: synthesis and characterization of Fe- and Al-MFI zeotypes. Topics Catal 62(7–11):689–698
27. Rouquerol J, Llewellyn P, Rouquerol F (2007) Is the bet equation applicable to microporous adsorbents? Stud Surf Sci Catal 160:49–56. https://doi.org/10.1016/S0167-2991(07)80008-5
28. Topsøe NY, Pedersen K, Derouane EG (1981) Infrared and temperature-programmed desorption study of the acidic properties of ZSM-5-type zeolites. J Catal 70(1):41–52. https://doi.org/10.1016/0021-9517(81)90315-8
29. van Koningsveld H, Jansen JC, van Bekkum H (1990) The monoclinic framework structure of zeolite H-ZSM-5. Comparison with the orthorhombic framework of as-synthesized ZSM-5. Zeolites 10(4):235–242
30. Hunger B, Heuchel M, Matysik S, Beck K, Einicke WD (1995) Adsorption of water on ZSM-5 zeolites. Thermochim Acta 269-270(C):599–611
31. Thommes, M. et al. Physisorption of gases, with special reference to the evaluation of surface area and pore size distribution (IUPAC Technical Report). Pure and Applied Chemistry **87** (9-10), 1051–1069 (2015). https://www.degruyter.com/document/doi/10.1515/pac-2014-1117/html. doi:10.1515/PAC-2014-1117
32. Alothman ZA (2012) A review: fundamental aspects of silicate mesoporous materials. Materials 5(12):2874–2902
33. Demmin RA, Gorte RJ (1984) Design parameters for temperature-programmed desorption from a packed bed. J Catal 90(1):32–39. https://doi.org/10.1016/0021-9517(84)90081-2
34. Derouane EG et al (2013) The acidity of zeolites: concepts, measurements and relation to catalysis: a review on experimental and theoretical methods for the study of zeolite acidity. Catal Rev 55(4):454–515
35. Rodríguez-González L et al (2007) The acid properties of H-ZSM-5 as studied by NH3-TPD and 27Al-MAS-NMR spectroscopy. Appl Catal A 328(2):174–182. https://doi.org/10.1016/J.APCATA.2007.06.003
36. Miyamoto T, Katada N, Kim JH, Niwa M (1998) Acidic property of MFI-type gallosilicate determined by

temperature-programmed desorption of ammonia. J Phys Chem B 102(35):6738–6745. https://doi.org/10.1021/jp980007r
37. Cheng YT, Huber GW (2011) Chemistry of furan conversion into aromatics and olefins over HZSM-5: a model biomass conversion reaction. ACS Catal 1(6):611–628. https://doi.org/10.1021/cs200103j
38. Arena F, Chio RD, Trunfio G (2015) An experimental assessment of the ammonia temperature programmed desorption method for probing the surface acidic properties of heterogeneous catalysts. Appl Catal A 503:227–236. https://doi.org/10.1016/J.APCATA.2015.05.035
39. Choi SW et al (2017) Propane dehydrogenation catalyzed by gallosilicate MFI zeolites with perturbed acidity. J Catal 345:113–123. https://doi.org/10.1016/J.JCAT.2016.11.017
40. Zhou Y et al (2020) Ethylene dehydroaromatization over Ga-ZSM-5 catalysts: nature and role of gallium speciation. Angew Chem Int Ed 59(44):19592–19601
41. Kim W et al (2017) Hierarchical Ga-MFI catalysts for propane dehydrogenation. Chem Mater 29 (17):7213–7222
42. McLellan GD, Howe RF, Parker LM, Bibby DM (1986) Effects of coke formation on the acidity of ZSM-5. J Catal 99(2):486–491. https://doi.org/10.1016/0021-95178690373-8
43. Uslamin EA, Kosinov NA, Pidko EA, Hensen EJM (2018) Catalytic conversion of furanic compounds over Ga-modified ZSM-5 zeolites as a route to biomass-derived aromatics. Green Chem 20(16):3818–3827. https://doi.org/10.1039/C8GC01528G
44. Otero Areán C, Turnes Palomino G, Geobaldo F, Zecchina A (1996) Characterization of gallosilicate MFI-type zeolites by IR spectroscopy of adsorbed probe molecules. J Phys Chem 100(16):6678–6690. https://doi.org/10.1021/jp952952a
45. Parrillo DJ, Lee C, Gorte RJ, White D, Farneth WE (1995) Comparison of the acidic properties of H- [Al]ZSM-5, H- [Fe]ZSM-5, and H- [Ga]ZSM-5 using microcalorimetry, hexane cracking, and propene oligomerization. J Phys Chem 99(21):8745–8749. https://doi.org/10.1021/j100021a046
46. Freitas C, Barrow NS, Zholobenko V (2018) Accessibility and location of acid sites in zeolites as probed by Fourier transform infrared spectroscopy and magic angle spinning nuclear magnetic resonance. Johnson Matthey Technol Rev 62(3):279–290. https://doi.org/10.1595/205651318X696792
47. Thibault-Starzyk F, Vimont A, Gilson JP (2001) 2D-COS IR study of coking in xylene isomerisation on H-MFI zeolite. Catal Today 70(1–3):227–241. https://doi.org/10.1016/S0920-5861(01)00420-5